

# Controlled synthesis of single-crystalline InN nanorods

Olga Kryliouk<sup>1,5</sup>, Hyun Jong Park<sup>1</sup>, Yong Sun Won<sup>1</sup>,  
Tim Anderson<sup>1</sup>, Albert Davydov<sup>2</sup>, Igor Levin<sup>2</sup>, Ji Hyun Kim<sup>1,3,4</sup>  
and Jaime A Freitas Jr<sup>4</sup>

<sup>1</sup> Chemical Engineering Department, University of Florida, Gainesville, FL 32611, USA

<sup>2</sup> Materials Science and Engineering Laboratory, NIST, Gaithersburg, MD 20899, USA

<sup>3</sup> Department of Chemical and Biological Engineering, Korea University, Seoul 136-701, Korea

<sup>4</sup> ESTD, Naval Research Laboratory, Washington, DC 20375, USA

E-mail: [olgak@grove.ufl.edu](mailto:olgak@grove.ufl.edu)

Received 4 December 2006, in final form 18 January 2007

Published 28 February 2007

Online at [stacks.iop.org/Nano/18/135606](http://stacks.iop.org/Nano/18/135606)

## Abstract

Single-crystalline InN nanorods were successfully grown on c-Al<sub>2</sub>O<sub>3</sub>, GaN, Si(111), and Si(100) substrates by non-catalytic, template-free hydride metal–organic vapour phase epitaxy (H-MOVPE). It was evaluated thermodynamically and confirmed experimentally that the domain of nanorod growth lies in the vicinity of the growth–etch transition. Stable gas phase oligomer formation is suggested as the nucleation mechanism for InN nanoparticle generation. Dislocation-free, high-quality InN nanorods with [00.1] growth axis were formed via an apparent solid–vapour growth mechanism. The nanorod diameter, density, and orientation were controlled by growth temperature, substrate selection, and HCl/TMIn and N/In inlet molar ratios.

 Supplementary data are available from [stacks.iop.org/Nano/18/135606](http://stacks.iop.org/Nano/18/135606)

## 1. Introduction

The group III nitrides have received considerable attention over the past decade as promising materials for optoelectronic and high-power, high-temperature electronic device applications [1–3]. Although most previous work has focused on GaN-based materials, InN is now under focus due to the wide variation in the reported bandgap energy and higher electron mobility. In particular, the reported value for the room temperature bandgap energy varies over the large range 0.6–0.8 [4–10] to 1.9 eV [11]. A critical review by Butcher and Tansley [12] presents a comprehensive analysis of the data and proposed models surrounding the bandgap controversy and concludes that the current analysis of InN is not yet sufficient to assign a bandgap value to the material. In addition to the uncertainty with the bandgap value, the routine growth of high-quality hexagonal InN films with a low background carrier concentration is not yet obvious.

Although most GaN-based films are deposited by MOVPE, this method must overcome certain challenges to

grow InN. In particular, the high thermal decomposition pressure of InN [13, 14] requires a low growth temperature (<700 °C). Based on our experience and consistent with published data [15, 16], indium droplet formation occurs in conventional MOVPE unless an extremely high (>50 000) NH<sub>3</sub>/TMIn ratio is used. Excess NH<sub>3</sub>, however, significantly reduces the InN growth rate as a result of reactions involving hydrogen, which is formed from NH<sub>3</sub> decomposition. This is consistent with the observation that InN annealed in NH<sub>3</sub> decomposes at a lower temperature than in N<sub>2</sub> [17]. Controlling the dimensions of any nanostructured material makes growth more challenging as compared to growth of a thin film. As expected for InN, reports on the growth and properties of InN one-dimensional (1D) materials are limited [18–31]. Controlled synthesis of InN and related materials not only opens the opportunity for fundamental studies but also for new applications in future electronic and photonic devices.

We have reported on the growth and characterization of high quality InN films by a modified version of hydride vapour phase epitaxy (HVPE) in which HCl is reacted with

<sup>5</sup> Author to whom any correspondence should be addressed.

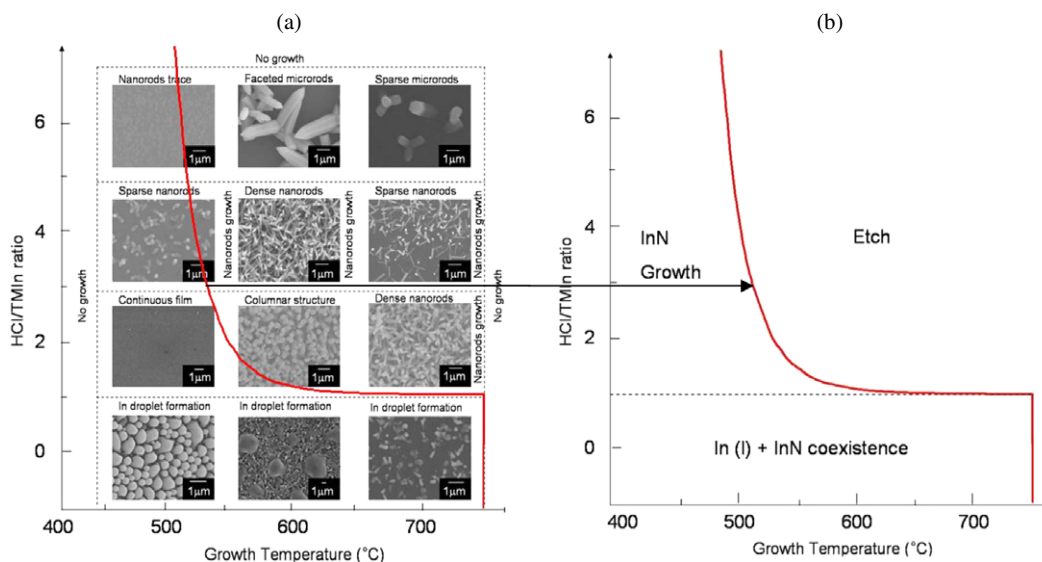


**Figure 1.** (a) H-MOVPE InN growth map: growth temperature versus HCl/TMIn at  $N/\text{In} = 250$ , substrate— $c\text{-Al}_2\text{O}_3$ . (b) Companion equilibrium CVD diagram: calculated growth/etch transition temperature as a function of HCl/TMIn ratio for  $N/\text{In} = 250$ .

(This figure is in colour only in the electronic version)

trimethyl indium (TMIn) instead of liquid In in the source zone [31]. This process is termed hydride metal organic vapour phase epitaxy (H-MOVPE). Based on experimental results supported by an equilibrium analysis, it was determined that single-phase InN (i.e. free from metallic indium) can be grown at a  $N/\text{In}$  ratio as low as 2500 by adding HCl to the inlet with a HCl/TMIn molar ratio in the range 0.3–1.4. An equilibrium analysis of the In–N–Cl–H–C system was performed to identify transition region between single phase InN deposition and co-deposition with In [28, 31]. Interestingly, growth of InN nanorods was observed to occur at conditions in the vicinity of the growth–etch transition [28].

Previous reports on the synthesis of 1D III nitrides have used catalyst- or template-assisted growth techniques [20–24]. In this study, single crystal InN nanorods (NRs) were successfully grown by non-catalytic, template-free H-MOVPE. The InN NRs were extensively characterized (described in supporting information available at [stacks.iop.org/Nano/18/135606](http://stacks.iop.org/Nano/18/135606)) by field emission scanning electron microscopy (FESEM), x-ray diffraction  $2\theta$ – $\omega$  scan, transmission electron microscopy (TEM), selected area electron diffraction (SAED), energy dispersive spectroscopy (EDS), Raman scattering spectroscopy, photoluminescence (PL), and cathodoluminescence (CL).

## 2. Experimental details

The InN NRs were grown using a horizontal, hot wall reactor (see supporting information figure 1S available at [stacks.iop.org/Nano/18/135606](http://stacks.iop.org/Nano/18/135606)). The detailed description of this system is presented elsewhere [32]. Trimethyl indium (solution TMIn<sup>TM</sup>) from Epichem and  $\text{NH}_3$  (99.999%) from Matheson Tri-Gas were used as In and N sources, respectively. In this process TMIn is first reacted with HCl in the source zone of the hot wall reactor to form chlorinated indium species. The stream is then combined with  $\text{NH}_3$  in the downstream mixing zone and directed towards a substrate where deposition

of InN occurs. The growth was performed at atmospheric pressure in  $\text{N}_2$  ambient. The growth conditions for this study were as follows: growth temperature in the range 400–700 °C; HCl/TMIn inlet mole ratio in the range 0–6;  $N/\text{In}$  ratio in the range  $10^2$ – $10^4$ ; and  $\text{N}_2$  carrier gas flow rate of 1.6 slm. A set of substrates  $c\text{-Al}_2\text{O}_3$ , GaN ( $5\ \mu\text{m}$ )/ $c\text{-Al}_2\text{O}_3$ , Si(111), and Si(100) were compared by loading all four into the reactor for a given run.

## 3. Results and discussion

It was determined that the HCl/TMIn ratio and growth temperature were the most important parameters for realizing InN NR deposition. The average nanorod diameter and density were controlled by growth temperature, and the HCl/TMIn and  $N/\text{In}$  ratios. A series of 56 growth runs were performed at seven different temperatures (400–700 °C in 50 °C increments) and eight different HCl/TMIn ratios (0, 1, 2, ..., 7). No growth was observed at 400 °C and only very limited growth at 450 °C. Figure 1(a) shows SEM images of representative samples grown on  $c\text{-Al}_2\text{O}_3$  at 500, 600, and 700 °C with HCl/TMIn = 0, 2, 4, and 6 and  $N/\text{In} = 250$ . The growth map shown in this figure provides clear directions for H-MOVPE growth of InN films and nano/microrods. It was observed in separate experiments that In droplet formation is unavoidable unless growth is performed in the chlorinating environment at values of HCl/TMIn  $\geq 0.3$ . A uniform InN film without indium droplet formation is grown at  $T < 600$  °C and relatively low HCl/TMIn ratio ( $< 2$ ). For HCl/TMIn ratio in the range 1–2 and temperature range 600–700 °C, polycrystalline and columnar InN films along with dense nanorods are observed. A low density of rods is grown at excessively high HCl/TMIn ratio (5–6) with NRs for  $T < 550$  °C, and microrods at  $T > 650$  °C. The relatively high HCl flow promotes a low density of nucleation sites, perhaps because of etching reactions, and a higher temperature

promotes larger nucleus size, possibly through aggregation of smaller nuclei. The conditions for growth of a high density of NRs are in the vicinity of  $T = 600^\circ\text{C}$ ,  $\text{N}/\text{In} = 250$ , and  $\text{HCl}/\text{TMIIn} = 4$ . Interestingly, these conditions leading to growth of high density InN NRs are near the growth–etch transition temperature as shown in figure 1(b) and described below.

As summarized above, the growth mode is sensitive to the  $\text{HCl}/\text{TMIIn}$  ratio and growth temperature. In the NR growth mode the density, diameter, and length are strongly dependent on these two parameters, while the NR diameter increases with increasing  $\text{N}/\text{In}$  ratio. A detailed morphological study of InN NRs is presented elsewhere [28]. It is noted in figure 1(a) that the diameter of an individual NR does not change along the growth direction. A nucleation mechanism that involves liquid In nano- or micro-dots is not supported by the microstructure map shown in figure 1(a). The nanorods do not show a different cap morphology, that would be expected from In solidification or lower rate InN formation that would occur upon cooling. Furthermore, the equilibrium analysis predicts that  $\text{In}(\text{l})$  will not form when the  $\text{HCl}/\text{TMIIn}$  ratio is greater than slightly above unity. Yet the NRs appear at very high values of this ratio. Although a detailed description of the self-nucleation and growth process is not known, these observations are consistent with a solid–vapour mechanism initiated by random nucleation of precursor species and the subsequent directional growth along the  $c$ -axis.

To better understand the growth conditions of InN nanorods, a complex chemical equilibrium analysis of the In–N–Cl–H–C–inert system was performed [31]. The boundary between growth and etch conditions for InN H-MOVPE growth was calculated using the *ThermoCalc* software with base conditions as  $P = 1$  atm,  $\text{N}/\text{In} = 250$ ,  $\text{C}/\text{In} = 3$ ,  $\text{Inert}/\text{In} = 2286$ , and the H atom fraction is given by  $x(\text{H}) = 9 * x(\text{In}) + x(\text{Cl}) + 3 * x(\text{N})$  with varying  $\text{Cl}/\text{In}$  ratio from 0 to 8 to duplicate the experimental conditions. The companion equilibrium CVD diagram is shown in figure 1(b). The growth/etch transition temperature decreases with increasing  $\text{HCl}/\text{TMIIn}$  ratio since the added Cl tends to retain In in the vapour phase as volatile  $\text{In}_x\text{Cl}_y$  species, and no  $\text{In}(\text{l})$  exists at  $\text{HCl}/\text{TMIIn} > 1$ . The general growth trend is consistent with the equilibrium predictions. The general agreement between experimental observations and conditions predicted to yield no net growth or etching suggests that operating near this transition allows for precise control of the nucleation process, and thus the opportunity to control the density and dimensions of the nanostructures. Once stable nuclei form on the substrate surface, epitaxial growth is expected for conditions of moderate lattice mismatch. One of the advantages of the H-MOVPE technique is the ability to vary the  $\text{Cl}/\text{In}$  input.

Based on these observations and a review of the more extensive GaN nanoparticle formation literature, it appears likely that nucleation of InN seeds involves gas-phase oligomer formation. Formation of stable gas-phase group III nitride oligomers during MOVPE has been examined using computational chemistry [33–39]. These studies concluded that spontaneous growth of amido  $(\text{DMGa}:\text{NH}_2)_n$  and imido  $(\text{CH}_3\text{Ga}:\text{NH})_n$  oligomers is thermodynamically favourable, and their nucleation should thermodynamically lead to the formation of GaN nanoparticles [35].

The detailed mechanism for seeding the NRs, however, is not known. As discussed above, a mechanism involving nano-sized liquid In is not suggested since In droplets are not present when the  $\text{HCl}/\text{TMIIn}$  ratio is  $>0.3$ , and a larger value is required experimentally to grow NRs. For our process, equilibrium calculations suggest that TMIIn should completely react with the inlet HCl in the source zone (temperature set at  $\sim 300^\circ\text{C}$ ) when the  $\text{HCl}/\text{TMIIn}$  ratio is  $>1$  to form  $\text{InCl}$  ( $1 < \text{Cl}/\text{In} < 2$ ) or  $\text{In}_2\text{Cl}_4$  ( $2 < \text{Cl}/\text{In} < 7$ ). This is consistent with observation of no In deposit on the inlet tube after a run (or InN formed by back-diffusion of  $\text{NH}_3$ ). The volatile  $\text{In}_x\text{Cl}_y$  stream is then mixed with  $\text{NH}_3$  and delivered to the deposition zone at the higher growth temperature where different reaction pathways lead to different surface morphologies.

From previous results [28, 31] and those reported here, the growth temperature of InN in any form is in the approximate range  $500^\circ\text{C} \leq T \leq 700^\circ\text{C}$ . When the  $\text{HCl}/\text{TMIIn}$  ratio is unity or slightly higher and in the low temperature range  $500^\circ\text{C} < T < 600^\circ\text{C}$ , 2D growth of InN occurs. The exact mechanism is unknown, but this growth process gives N-terminated polarization and thus an Ely-Rideal [40] reaction of  $\text{NH}_3$  with adsorbed  $\text{InCl}$  ( $\text{InCl}(\text{adsorbed}) + \text{NH}_{3\text{g}} \rightarrow \text{InN}_s + \text{HCl}_g + \text{H}_{2\text{g}}$ ) might be a possible mechanism. It is also possible that reversible formation/dissociation of an adduct with  $\text{NH}_3$  could also play a role.

At higher temperature ( $600^\circ\text{C} \leq T \leq 700^\circ\text{C}$ ) and high  $\text{HCl}/\text{TMIIn}$  ratio ( $\geq 1$ ), columnar structures are observed with varying diameter (micro, nano) and density. As shown in the CVD diagram, there can be variation in the rod-to-rod diameter for a given run, but the diameter of a single rod does not vary in the growth direction, which is the along  $c$ -axis. This 1D growth habit implies the diameter is fixed by the dimension of the nuclei. At these higher temperatures, it is possible that oligomers formed in the gas phase adsorb on the surface, cluster, and produce nuclei for columnar growth. Quantum chemical calculations of the reversible formation of the ammonia adduct ( $\text{GaCl}_3:\text{NH}_3$ ) and the subsequent formation of the amido ( $\text{Cl}_2\text{GaNH}_2$ ) and imido ( $\text{ClGaNH}$ ) monomers via successive HCl elimination leads to direct formation of Ga–N bonds [38]. The calculations suggest that chains and cyclic oligomers are thermodynamically favoured in the temperature range of this study. The oligomerization is promoted by the strong intramolecular H–Cl hydrogen bonding and dipole–dipole interactions. The chemistry of In adduct formation with  $\text{NH}_3$  and oligomer formation is expected to be similar to that for Ga [36].

Experimentally, the diameter increases with added  $\text{NH}_3$  while holding other growth conditions constant [31]. This is consistent with added  $\text{NH}_3$  driving the oligomerization reaction to longer chain length to yield larger diameter nuclei. Alignment of the oligomers on the substrate for directional growth along the  $c$ -axis is facilitated by dipole–dipole interactions between the natural polarization in wurtzite InN along the  $c$ -axis and the strong dipole moments in chlorine-containing reactants (such as unconverted  $\text{InCl}$  and/or  $\text{Cl}_2\text{InNH}_2$ ) and  $\text{NH}_3$ . The proposed mechanism is speculative and more detailed studies on the nucleation and growth mechanism are needed.

A representative FESEM plane-view image of InN nanorods grown on Si(111) is shown in figure 2(a). Nanorods

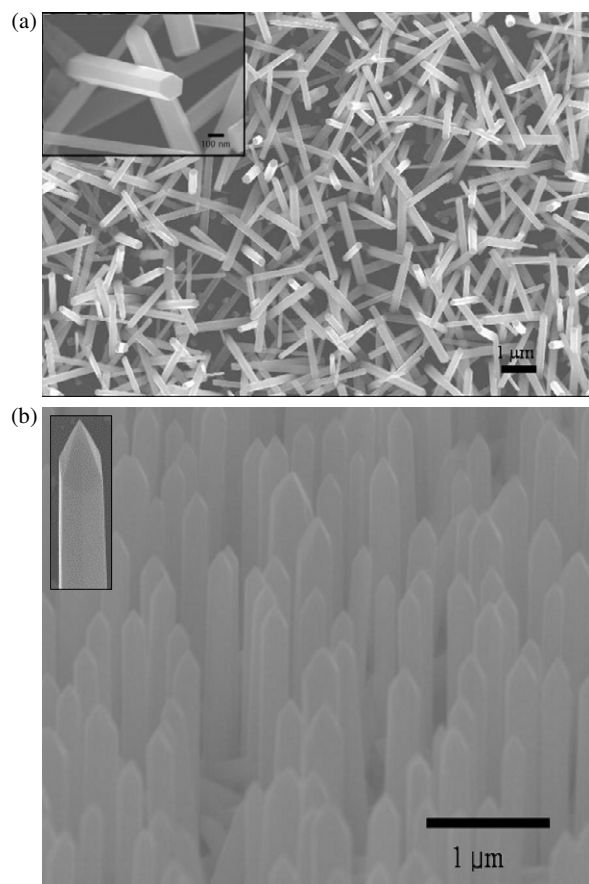


**Figure 2.** SEM image of InN nanorods grown on Si(111) (a) and GaN (b) at  $T = 600^\circ\text{C}$ ,  $\text{Cl/III} = 4$ ,  $\text{N/In} = 250$ , growth time = 1 h.

grown at the conditions specified in the caption were textured in the  $[00.1]$  direction with typical diameters in the range 50–400 nm and lengths of  $\sim 1 \mu\text{m}$  for 1 h growth time. The well defined hexagonal cross-section of the nanorods is clearly observed in the figure 3(a) inset. Based on the XRD  $2\theta$  scan of InN NRs grown on  $c\text{-Al}_2\text{O}_3$  (figure 2Sa available at [stacks.iop.org/Nano/18/135606](http://stacks.iop.org/Nano/18/135606)) all detected reflections correspond to the wurtzite structure of InN (PDF 02-1450). It was found, however, that the nanorods were not randomly oriented as compared to the powder pattern shown in figure 2Sc available at [stacks.iop.org/Nano/18/135606](http://stacks.iop.org/Nano/18/135606). Comparing the InN powder pattern (PDF 02-1450, figure 2Sc available at [stacks.iop.org/Nano/18/135606](http://stacks.iop.org/Nano/18/135606)) to the nanorods, it was concluded that the intensity of the InN(002) peak was consistently higher than the InN powder pattern, regardless of the substrate type. This is an indication that InN nanorods are highly textured in the  $[00.1]$  direction.

Interestingly, changing the substrate from  $c\text{-Al}_2\text{O}_3$  or either Si orientation to GaN ( $5 \mu\text{m}$ )/ $c\text{-Al}_2\text{O}_3$  resulted in the growth of self-aligned  $(00.1)$ -oriented arrays of InN nanorods as shown in figure 3(b). The interface between the InN and GaN layer is clearly epitaxial with the  $[00.1]$  InN nanorod and  $[00.1]$  GaN/ $c\text{-Al}_2\text{O}_3$  relationship. An XRD  $2\theta$ - $\omega$  scan of self-aligned InN nanorods showed only (002) and (004) InN peaks (figure 2Sb available at [stacks.iop.org/Nano/18/135606](http://stacks.iop.org/Nano/18/135606)). The mechanism for nanorod self-alignment has yet to be established.

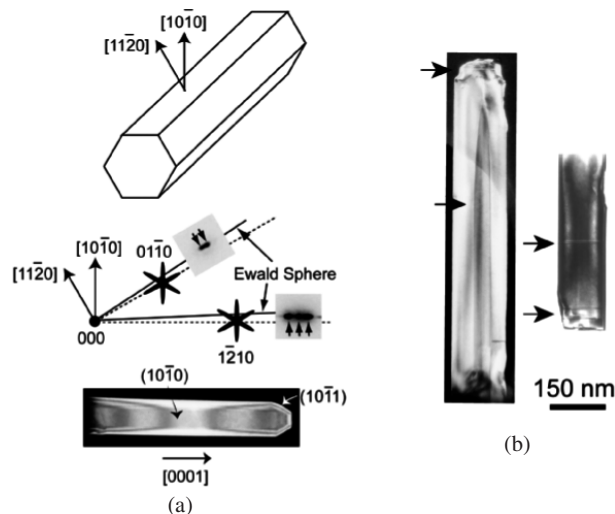


**Figure 3.** (a) Top—schematic drawing of the InN nanorods with the orientation of the nanorods habits indicated. Middle—splitting of the  $01\bar{1}0$  and  $1210$  reflections (insets) in the  $[11\bar{2}0]$  and  $[10\bar{1}0]$  zone axis electron diffraction patterns, respectively, of the single NR. The schematic drawings illustrate that the splitting results from the intersection of the Ewald sphere with the three streaks of intensity passing through each reflection. Bottom—dark-field TEM image of the InN nanorods recorded close to the  $[10\bar{1}0]$  orientation. A faceting on the  $(10\bar{1}1)$  planes at the NR tip is observed. (b) Dark-field images of the InN NR revealing occasional planar defects.

The structural quality of InN nanorods was analysed using TEM as shown in figures 3(a) and (b). The inset in figure 3(a) shows splitting of reflections in the  $(10.0)$  and  $(11.0)$  selected area electron diffraction patterns. The schematic diagrams illustrate that the splitting results from the intersection of the Ewald sphere with the streaks of the diffracting intensity extending through each reflection. The three streaks in reciprocal space, which originate from the well defined hexagonal shape of the nanorod, are perpendicular to the NR facets. Depending on the zone axis orientation, the Ewald sphere intersects either two or three streaks, thus enabling determination of the facet plane. A bright-field (BF) image of the NR is presented at the bottom of figure 3(a). Electron diffraction patterns (not shown here) confirmed that the nanorods are single crystalline with the  $[00.1]$  growth axis and  $\{10.0\}$  facet planes (see figure 3(a)). It is interesting to note that this type of faceting appears to be different from faceting in wurtzite ZnO nanorods, where facets were found to predominantly reside on the  $\{11.0\}$  planes [41, 42]. TEM also showed that the shape of nanorod tips is affected by growth conditions: nanorods exhibited either flat top (not shown here but similar to the FESEM image in figure 2(a) inset) or pyramid-truncated shape (figure 3(a)) with side facets residing on  $\{10.1\}$  planes. Dark- and bright-field images (figure 3(b)) revealed that nanorods were dislocation free with sparse planar defects. These defects extended across individual nanorods and can be attributed to stacking faults residing on  $\{00.1\}$  planes.

The EDS analysis shows no contamination of nanorods with chlorine, carbon, or oxygen. The EDS line-scan of an individual InN nanorod grown on GaN substrate as seen in figure 3S available at [stacks.iop.org/Nano/18/135606](http://stacks.iop.org/Nano/18/135606) clearly shows that it consists of indium and nitrogen.

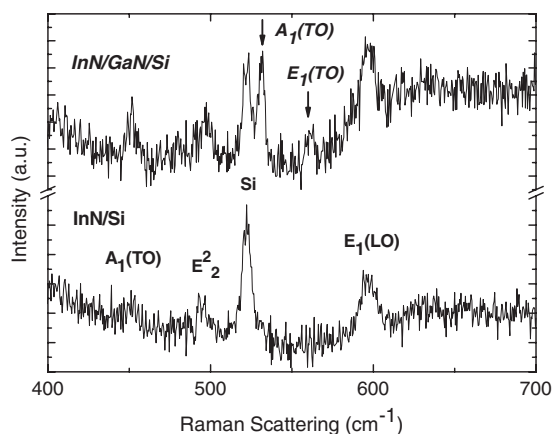


**Figure 4.** Room-temperature Raman scattering of InN nanorods deposited on Si and GaN/Si substrates at  $T = 600^\circ\text{C}$ , Cl/III = 4, N/In = 250, growth time = 1 h.

Raman scattering is a well established non-destructive technique to study vibrational phenomena in solids. Since inelastic light scattering in crystals is susceptible to selection rules, this technique can be conveniently used to identify crystalline structures and evaluate material quality and composition. Similar to AlN and GaN, InN crystal with 2H (wurtzite) structure belongs to the space group  $C_{6v}^4$  and has two molecules per unit cell. Group theory predicts eight zone-centre optical phonons, namely  $1A_1$  (transversal optical (TO)),  $1A_1$  (longitudinal optical (LO)),  $2B_1$  (optically inactive or 'silent'),  $1E_1$  (TO),  $1E_1$  (LO), and  $2E_2$ .

The first-order Raman spectrum of InN NRs deposited directly on Si substrate is shown in the bottom spectrum of figure 4. Three phonon lines are clearly observed, despite the noise, at 451, 496, and 596  $\text{cm}^{-1}$ , which are assigned to  $A_1$ (TO),  $E_2^2$ , and  $E_1$ (LO), respectively. The line at 522  $\text{cm}^{-1}$  is the first-order phonon of the Si substrate. The measured phonon energy values are between 3 and 8  $\text{cm}^{-1}$  larger than the values reported in the literature [43, 44]. These shifts may result from stress and/or heat reduction, due to the sample morphology and experimental conditions, respectively. It was observed that measurements performed with a small laser spot and higher laser power resulted in sample damage. It was also observed that the  $E_2^2$  phonon is more susceptible to stress, consistent with the larger energy difference reported in the present work [45]. The different relative intensities of the observed phonon lines, as compared with reported data, do not result from breaking of the selection rules, but from the random orientation of the nanorods. A typical Raman spectrum of the InN NRs deposited on GaN/Si(111) is represented in the top spectrum of figure 4. Note the similarity of both spectra, with the exception of the additional lines at 531 and 561  $\text{cm}^{-1}$ , which are assigned to the GaN phonons  $A_1$ (TO) and  $E_1$ (TO), respectively. The sharpness of the InN lines is consistent with good crystalline quality of the nanorods. RT PL maximum emission was observed at  $\sim 0.9\text{--}0.95$  eV while the low-temperature (7 K) CL peak was detected at 0.89 eV.

#### 4. Conclusion

In conclusion, high-quality, single-crystal InN nanorods were grown by a non-catalytic H-MOVPE technique. The growth

morphology was mapped as a function of growth conditions and it was observed that the diameters and the densities of the nanorods depend strongly on the growth temperature and the N/In and HCl/TMIn ratios. The experimental results are consistent with the suggestion that oligomerized species are involved in the nucleation step for the growth of nanostructured InN. The results suggest that H-MOVPE is a promising technique for the fabrication of nanostructured materials. Since this growth method uses no catalyst or nano-template, it could be extended for the growth of other III nitrides, such as GaN, AlN, and their solid solutions, such as  $\text{In}_x\text{Ga}_{1-x}\text{N}$  and  $\text{Al}_x\text{Ga}_{1-x}\text{N}$ .

#### Acknowledgments

The work at UF was partially supported by the US Army, grant FA 8650-04-2-1619. The authors would like to thank the staff at the Microfabritech and Major Analytical Instrumentation Center, University of Florida.

JAF and J-HK were partially supported by ONR contract N0001405WR20317 and NRL contract N000173-05-1G01.

#### References

- [1] Matsuoka T 2005 *Superlatt. Microstruct.* **37** 19–32
- [2] Ruterana P, Albrecht M and Neugebauer J (ed) 2003 *Nitride Semiconductors: Handbook on Materials and Devices* (Weinheim: Wiley-VCH)
- [3] Ambacher O 1998 *J. Phys. D: Appl. Phys.* **31** 2653–710
- [4] Davydov V Yu *et al* 2002 *Phys. Status Solidi b* **229** R1–3
- [5] Bechstedt F and Furthmüller J 2002 *J. Cryst. Growth* **246** 315–9
- [6] Laakso A, Oila J, Kemppinen A, Saarinen K, Egger W, Liskay L, Sperr P, Lu H and Schaff W J 2004 *J. Cryst. Growth* **269** 41–9
- [7] Inushima T, Mamutin V V, Vekshin V A, Ivanov S V, Sakon T, Motokawa M and Ohoya S 2001 *J. Cryst. Growth* **227/228** 481–5
- [8] Higashiwaki M and Matsui T 2004 *J. Cryst. Growth* **269** 162–6
- [9] Vurgaftman I and Meyer J R 2003 *J. Appl. Phys.* **94** 3675–96
- [10] Goldhahn R *et al* 2004 *Superlatt. Microstruct.* **36** 591–7
- [11] Tansley T L and Foley C P 1984 *Electron. Lett.* **20** 1066–8
- [12] Butcher K S A and Tansley T L 2005 *Superlatt. Microstruct.* **38** 1–37
- [13] Ambacher O *et al* 2002 *J. Phys.: Condens. Matter* **14** 3399–434
- [14] Onderka B, Unland J and Schmid-Fetzer R 2002 *J. Mater. Res.* **17** 3065–83
- [15] Kumagai Y, Kikuchi J, Matsuo Y, Kangawa Y, Tanaka K and Koukita A 2004 *J. Cryst. Growth* **272** 341–7
- [16] Matsuoka T, Okamoto H, Nakao M, Harima H and Kurimoto E 2002 *Appl. Phys. Lett.* **81** 1246–8
- [17] Drago M, Schmidting T, Werner C, Pristovsek M, Pohl U W and Richter W 2004 *J. Cryst. Growth* **272** 87–93
- [18] Briot O, Maleyre B, Ruffenach S, Pinquier C, Demangeot F and Frandon J 2003 *Phys. Status Solidi c* **7** 2851–4
- [19] Dimakis E, Konstantinidis G, Tsagaraki K, Adikimenakis A, Iliopoulos E and Georgakilas A 2004 *Superlatt. Microstruct.* **36** 497–507
- [20] Tang T, Han S, Jin W, Liu X, Li D C, Zhang D, Zhou C, Chen B, Han J and Meyyapan M 2004 *J. Mater. Res.* **19** 423
- [21] Lan Z H, Wang W M, Sun C L, Shi S C, Hsu C W, Chen T T, Chen K H, Chen C C, Chen Y F and Chen L C 2004 *J. Cryst. Growth* **269** 87–94

- [22] Zhang J, Zhang L, Peng X and Wang X 2002 *J. Mater. Chem.* **12** 802–4
- [23] Liang C H, Chen L C, Hwang J S, Chen K H, Hung Y T and Chen Y F 2002 *Appl. Phys. Lett.* **81** 22–4
- [24] Johnson M C, Lee C J, Bourret-Courchesne E D, Konsek S L, Aloni S, Han W Q and Zettl A 2004 *Appl. Phys. Lett.* **85** 5670–2
- [25] Shih C F, Chen N C, Chang P H and Liu K S 2005 *J. Cryst. Growth* **281** 328–33
- [26] Zhang J, Xu B, Jiang F, Yang Y and Li J 2005 *Phys. Lett. A* **337** 121–6
- [27] Kryliouk O, Park H J, Wang H T, Kang B S, Anderson T J, Ren F and Pearton S J 2005 *J. Vac. Sci. Technol. B* **23** 1891–4
- [28] Park H J, Kang S W, Kryliouk O and Anderson T 2006 *Mater. Res. Symp. Proc.* **882** FF11-09.1–6
- [29] Chang C-Y, Chi G C, Wang W-M, Chen L-C, Chen K-H, Ren F and Pearton S J 2005 *Appl. Phys. Lett.* **87** 093112
- [30] Cheng G, Stern E, Turner-Evans D and Reed M 2005 *Appl. Phys. Lett.* **87** 253103
- [31] Park H J, Kryliouk O, Anderson T, Khokhlov D and Burbaev T 2006 *Physica E* at press (doi:10.1016/j.physe.2006.06.022)
- [32] Kryliouk O, Reed M, Dann T, Anderson T and Chai B 1999 *Mater. Sci. Eng. B* **59** 6–11
- [33] Karpov S Yu 2003 *J. Cryst. Growth* **248** 1–7
- [34] Averyanova M V, Przhevalskii I N, Karpov S Yu, Makarov Yu N, Ramm M S and Talalaev R A 1997 *Mater. Sci. Eng. B* **43** 167–71
- [35] Timoshkin A Y and Schaefer H F 2004 *J. Am. Chem. Soc.* **126** 12141–54
- [36] Okamoto Y 1998 *J. Cryst. Growth* **191** 405–12
- [37] Timoshkin A Y, Bettinger H F and Schaefer H F III 2002 *Inorg. Chem.* **41** 738–47
- [38] Kovacs A 2002 *Inorg. Chem.* **41** 3067–75
- [39] Cardelino B H, Moore C E, Cardelino C A, Frazier D O and Bachmann K J 2001 *J. Phys. Chem. A* **105** 849–68
- [40] Tamaru K D (ed) 1978 *Heterogeneous Catalysis* (London: Academic)
- [41] Levin I, Davydov A V, Nikoobakht B, Sanford N A and Mogilevsky P 2006 *Appl. Phys. Lett.* **87** 103119
- [42] Ding Y, Gao P X and Wang Z L 2004 *J. Am. Chem. Soc.* **126** 2066–72
- [43] Davydov V Yu, Emtsev V V, Goncharuk I N, Sminov A N, Petrikov V D, Mamutin V V, Vekshin V A, Ivanov S V, Smirnov M B and Inushima T 1999 *Appl. Phys. Lett.* **75** 3297–9
- [44] Chen J W, Chen Y F, Lu H and Schaff W J 2005 *Appl. Phys. Lett.* **87** 041907
- [45] Kim J-H, Freitas J A Jr, Klein P B, Jang S, Ren F and Pearton S J 2005 *Eleetrochem. Solid State Lett.* **8** G345–7